Article

^{68}Ga-Labeled Peptide for Noninvasive Quantifying Tumor Exposure of PD-L1 Therapeutics

Hui Nie, Lei Peng, Tianhong Yang, Junyu Chen, Chengde Xie, Lingyu Xue, Dake Zhang, Renbo Wu, Xiangsong Zhang,* and Zhihao Zha*

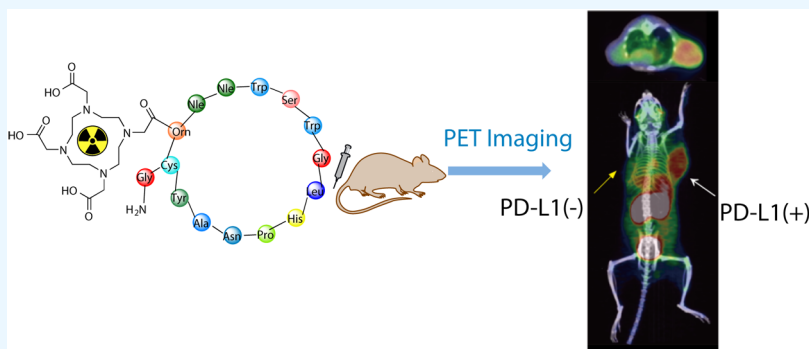Cite This: *ACS Omega* 2025, 10, 12495−12504

Read Online

ACCESS | Metrics & More | Article Recommendations | Supporting Information

PET Imaging
PD-L1(−)   PD-L1(+)

ABSTRACT: Purpose: Targeting the programmed death protein 1/programmed death-ligand 1 (PD-1/PD-L1) immune checkpoint blockade therapy plays a critical role in cancer therapy. However, not all patients benefit from this approach, with PD-L1 expression levels being a significant contributing factor. Positron emission tomography (PET) imaging of PD-L1 offers a noninvasive, whole-body, and dynamic assessment of its expression. This study aims to develop a novel peptide-based PD-L1 tracer, [^{68}Ga]HF12, to quantitatively evaluate PD-L1 expression in tumors, thereby offering clinical guidance. Methods: HF12 was successfully synthesized and radiolabeled with ^{68}Ga to yield [^{68}Ga]HF12. *In vitro* binding assays confirmed the specific binding affinity of HF12 for PD-L1 using CHO-hPD-L1 and CHO cell lines. Subsequent *in vivo* positron emission tomography (PET) imaging and biodistribution studies assessed [^{68}Ga]HF12 for monitoring PD-L1 expression levels in tumor-bearing mice, including those subjected to immunotherapy. Furthermore, PD-L1 expression in tumor tissues was evaluated by using autoradiography, Western blotting, and immunohistochemical (IHC) analysis. Results: The synthesis of [^{68}Ga]HF12 was successfully achieved with a radiochemical purity and yield exceeding 95%. Cellular uptake studies indicated that [^{68}Ga]HF12 demonstrated both high specificity and significant uptake in PD-L1-positive CHO-hPD-L1 cells. Micro-PET imaging and biodistribution studies revealed that [^{68}Ga]HF12 was preferentially accumulated in CHO-hPD-L1 tumors compared to PD-L1-negative CHO tumors. Treatment with Atezolizumab resulted in a significant reduction in [^{68}Ga]HF12 uptake in CHO-hPD-L1 tumors relative to pretreatment levels, whereas no significant changes were observed in the phosphate-buffered saline (PBS) control group. Subsequent biodistribution studies, along with Western blotting and immunohistochemical analyses, confirmed that PD-L1 expression levels in tumors were reduced following immunotherapy, consistent with the results obtained from PET imaging. Conclusions: [^{68}Ga]HF12 was successfully synthesized as a radiotracer for noninvasive quantitative PET imaging of PD-L1 expression levels. This radiotracer exhibited the potential to quantify PD-L1 expression across various tumors, thereby facilitating the prediction of patient response to anti-PD-1 and anti-PD-L1 immunotherapies and monitoring therapeutic efficacy.

■ INTRODUCTION

Tumor immune escape represents a critical mechanism for tumor occurrence and progression.[1] Immunotherapeutic strategies aimed at counteracting immune escape function by enhancing the body's ability to recognize and eradicate tumor cells through the inhibition of negative immune regulatory pathways.[2]

The programmed death protein 1/programmed death-ligand 1 (PD-1/PD-L1) interaction is a critical checkpoint that tumors exploit to evade immune surveillance. Inhibitors like
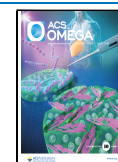
Nivolumab and Pembrolizumab have shown remarkable clinical efficacy, yet their benefits are confined to a substantial number of patients.[3,4] Studies have demonstrated a significant

correlation between PD-L1 expression levels and patient prognosis, particularly in the context of immunotherapy. This underscores the importance of accurately assessing PD-L1 expression to identify potential responders, monitor the efficacy of therapeutic interventions, and evaluate prognosis.[5,6]

Immunohistochemistry (IHC) is the clinical standard for assessing PD-L1 expression, but it faces challenges due to tumor heterogeneity, variable staining thresholds, and the impracticality of conducting serial biopsies to monitor dynamic changes in PD-L1 levels.[7,8] These limitations have spurred the development of noninvasive molecular imaging modalities that could potentially overcome these constraints.

Molecular imaging techniques, such as single photon emission computed tomography (SPECT) and positron emission tomography (PET), provide real-time, dynamic, noninvasive, and quantitative detection of PD-L1 expression throughout the body.[9] These significant advantages offer a novel avenue for evaluating PD-L1 levels in patients and for selecting candidates for immunotherapy.[10,11]

Current research identifies several types of PD-L1 radiotracers, including antibodies, antibody fragments, nanobodies, peptides, and small molecules.[12] For example, Bensch et al. utilized the positron-emitting radionuclide ^{89}Zr to label the PD-L1 inhibitory monoclonal antibody Atezolizumab, observing variable uptake across tumors and among patients. This variability may be attributed to the heterogeneous expression of PD-L1, suggesting that [^{89}Zr]Atezolizumab could serve as a noninvasive PET imaging agent for assessing PD-L1 levels.[13−15] However, the large molecular size of monoclonal antibodies often results in slow biodistribution, prolonged circulation times, and limited tissue penetration, typically requiring several days post-injection to achieve high-contrast imaging.[16−18] Additionally, the production of antibodies is complex, costly, and time-intensive compared to peptide synthesis.[19]

In contrast, peptides possess several advantages, including smaller molecular size, rapid clearance from the bloodstream and nontarget tissues, and effective tumor penetration, allowing for imaging within hours post-injection.[19,20] Sridhar Nimmagadda et al. identified a PD-L1 specific ligand, WL12, which was conjugated to the bifunctional chelator DOTAGA and radiolabeled with ^{64}Cu. This research demonstrated that [^{64}Cu]WL12 effectively detects varying PD-L1 expression levels in tumors, exhibiting high affinity and specificity along with rapid blood clearance.[21,22] Yang et al. were the first to apply [^{68}Ga]NOTA-WL12 in human imaging for nonsmall cell lung cancer patients, confirming its safety and effectiveness in quantifying in vivo PD-L1 expression and its potential to guide clinical selection for immunotherapy.[20] Building on this work, Nimmagadda et al. developed novel peptide-based PET radiotracers, [^{18}F]DK222 and [^{68}Ga]DK223, by modifying PD-L1 specific cyclic peptide DK221. These tracers produced high-contrast PET images within minutes of injection and demonstrated the capability to quantify dynamic changes in PD-L1 expression following immunotherapy.[23−25] Despite these advancements, no radiotracer has yet received Food and Drug Administration (FDA) approval for clinical use, underscoring the need for further development of peptide-based radiotracers with enhanced biological properties to inform clinical PD-L1 assessment.[26]

In this study, we designed and synthesized a novel peptide-based radiotracer, [^{68}Ga]HF12, to quantify PD-L1 expression and monitor changes in PD-L1 levels following immunother-apy. This radiotracer exhibited high affinity and specificity, allowing for high-contrast imaging of PD-L1 shortly after injection, and was primarily cleared via the kidneys. We conducted in vitro and in vivo assessments of [^{68}Ga]HF12, evaluating its biodistribution and PD-L1 targeting capabilities. Furthermore, we examined the ability of [^{68}Ga]HF12 to track dynamic changes in PD-L1 expression levels following treatment with monoclonal antibody Atezolizumab.

■ MATERIALS AND METHODS

General. All chemicals used were commercially available and were employed without further purification unless otherwise specified. The synthesis route for compound HF12 (cyclo(AcTyr-MeAla-Asn-Pro-His-Leu-MeGly-Trp-Ser-Trp-MeNle-MeNle-Orn-Cys)-Gly-NH$_2$) is detailed in the Supporting Information and was analyzed using high-performance liquid chromatography (HPLC) and online electrospray ionization (ESI) mass spectrometry (LC-MS, Waters, Milford, MA, USA). [^{68}Ga]GaCl$_3$ was eluted with 0.05 N hydrochloric acid (HCl) from a ^{68}Ge/^{68}Ga generator (ITG, Germany). The radioanalysis was performed using Agilent 1260 Infinity II HPLC (Palo Alto, USA) with a ZORBAX SB-C18 column (5 μm, 4.6 mm × 250 mm). The radioactivity was detected with a WIZARD 2480 γ-counter (PerkinElmer, USA). Micro-PET imaging was performed on Inveon PET scanner (Siemens, Germany).

Radiolabeling and Purification of [^{68}Ga]HF12. ^{68}Ga was eluted from the ^{68}Ge/^{68}Ga generator using 0.05 N HCl. In a reaction vessel, 10 μg of HF12 was dissolved in dimethyl sulfoxide (DMSO). Subsequently, 0.5 N sodium acetate buffer was added, followed by the introduction of 0.5 mL of a 0.05 N HCl solution containing [^{68}Ga]GaCl$_3$. The pH of the mixture was adjusted to 3.5−4.0, followed by heating at 95 °C for 10 min. The radiochemical yield and purity of [^{68}Ga]HF12 were evaluated by radio-HPLC (Table S1).

Cell Culture and Xenograft Models. Chinese hamster ovary cell line CHO-K1 (CHO) and human PD-L1 gene-transfected CHO-K1 cells (CHO-hPD-L1) were provided by Puzhou Gene Technology (Guangzhou, China). CHO and CHO-hPD-L1 were cultured in F-12K medium containing 10% fetal bovine serum (FBS, Gibco, USA) and 1% penicillin−streptomycin solution (P/S) at 37 °C in a 5% CO$_2$ atmosphere.

All animal experiments were performed according to the protocols approved by the First Affiliated Hospital of Sun Yat-sen University's Institutional Animal Care and Use Committee. NOD/SCID female mice, aged 6−8 weeks, were purchased from GemPharmatech Co., Ltd. The mice were group-housed in individually ventilated cages (3−5 mice per cage) at 25 °C with a 12 h light−dark cycle.

Following a 2-week acclimatization period, the mice were subcutaneously implanted on opposite sides of the axilla with 1.0×10^6 CHO-hPD-L1 and CHO cells, suspended in 100 μL of phosphate-buffered saline (PBS). The mice were subsequently available for PET imaging, biodistribution studies, and immunotherapy evaluations once tumor volumes reached 50−200 mm^3.

In Vivo **and** ***In Vitro*** **Stability.** [^{68}Ga]HF12 was incubated in PBS or FBS at 37 °C for various durations (1 and 2 h). At each time point, the radiochemical purity of 0.74 MBq sample was assessed using radio-HPLC. For the assessment of in vivo stability, female Kunming mice were administered intravenous injections of [^{68}Ga]HF12. At 15 min post-injection, blood
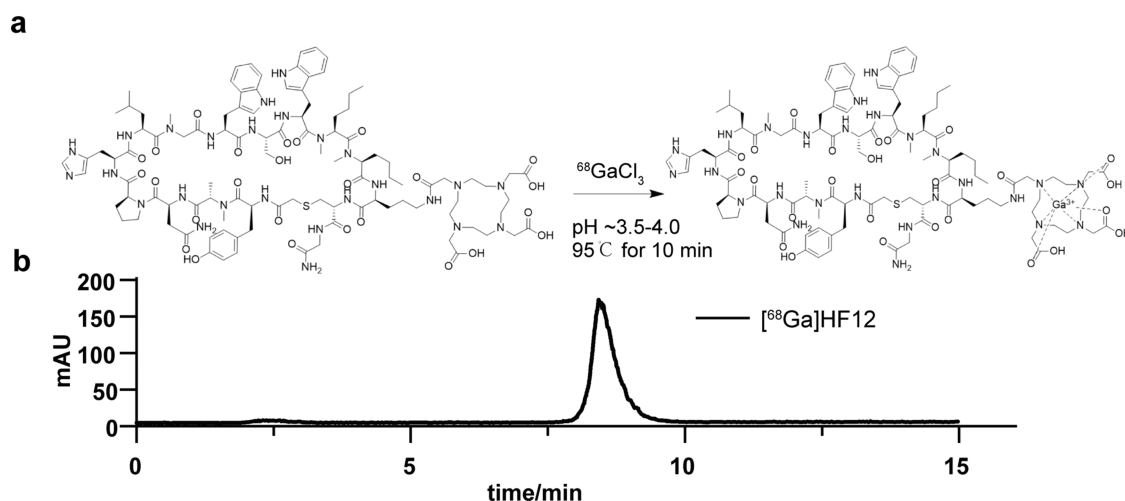
Figure 1. (a) Schematic diagram of the synthesis of radioactive tracer [68Ga]HF12. (b) HPLC analysis results of [68Ga]HF12.

samples were harvested, mixed with an equal volume of acetonitrile, and centrifuged at 10,000 rpm for 5 min. The supernatant was subsequently filtered, and the filtrate was analyzed using radio-HPLC to assess the purity of radiotracer.

Partition Coefficient. The radiotracers were added to equal volumes of *n*-octanol and PBS buffer, sealed, and vortexed for 2 min. Subsequent centrifugation was performed at 1200 rpm for 5 min. Equal volumes of the n-octanol and aqueous phases were extracted for measurement using an automatic γ-counter. The $\log P$ value was calculated as the logarithm of the radioactivity ratio between the octanol and the water phases.

Cell Uptake and Binding Assays. Various cancer cells (1×10^6), including CHO and CHO-hPD-L1, were seeded into 24-well plates and incubated for 24 h in F-12k medium supplemented with 10% FBS at 37 °C and 5% CO$_2$. Subsequently, the cells were treated with [68Ga]HF12 (74 kBq/well) at 37 °C for various durations. Following incubation, the cells were washed twice with cold PBS (pH 7.4) and lysed in 1 M sodium hydroxide (NaOH). For the blocked group, 30 μM PD-L1 inhibitor BMS1166 was co-incubated with CHO-hPD-L1 or CHO cells. The results were expressed as the percentage of radioactivity per 100 μg of protein. Competitive binding assays were performed by adding varying concentrations ($10^{-3}-10^4$ nM) of HF12 to each well containing 74 kBq of [68Ga]HF12. After the removal of the culture medium, the cells were washed twice with cold PBS, followed by lysis. The radioactivity of the lysed samples was quantified by using γ-counting.

Micro-PET Imaging. Following the intravenous administration of [68Ga]HF12 *via* the tail vein in xenograft models, static PET scans of 10 min and dynamic PET scans of 120 min were conducted. Regions of interest (ROIs) were delineated on the reconstructed images, with quantitative results reported as the percentage of injected dose per gram of tissue (%ID/g). In the inhibition studies, a static whole-body PET scan was conducted 60 min after coadministration of 50 μg of HF12 with the radiotracer. The dynamic imaging data were reconstructed into 12 frames using the OSEM3D algorithm. ROIs were then delineated using the Inveon Research Workplace software to generate the images.

Biodistribution Studies. To investigate the biodistribution of [68Ga]HF12, tumor-bearing mice were euthanized at specified time intervals post-injection. The organs of interest were collected, weighed, and analyzed with an automatic γ-counter. The result is presented as the percentage of injected dose per gram of tissue (%ID/g). To ascertain specificity, a separate cohort of mice was co-injected with 50 μg of the precursor along with the radiotracer.

Monitoring the Efficacy of Monoclonal Antibody Treatment. Tumor-bearing mice were randomly assigned to two groups: one treated with PBS (Group A, $n = 3$) and the other receiving the anti-PD-L1 antibody Atezolizumab (Group B, $n = 3$) *via* tail vein injection. During the treatment monitoring phase, PBS or Atezolizumab (10 mg/kg) was administered every 3 days for a total of five doses over a 14-day cycle. Tumor volumes and mouse body weights were recorded. End point criteria included a tumor volume exceeding 1500 mm^3 or a maximum tumor diameter greater than 20 mm. PET/computed tomography (CT) imaging was conducted before and after the treatment regimen. After the final treatment, a comprehensive evaluation of the monoclonal antibody was conducted, including biodistribution studies, Western blotting analysis, immunohistochemistry, and toxicity assessments.

Quantification of PD-L1 Expression. Cell pellets and frozen tumor tissues were lysed on ice for 10 min using a robust radioimmunoprecipitation assay (RIPA) lysis buffer to extract proteins, which were subsequently analyzed through gel electrophoresis to assess PD-L1 expression levels. In xenograft models, after administration of [68Ga]HF12, tumor tissues were harvested and sectioned. These sections were exposed to a phosphor screen and imaged using a Beckman Coulter FLA7000IP Typhoon phosphor imager. Immunohistochemical staining for PD-L1 was performed on adjacent tissue sections.

Statistical Analysis. Data are presented as the mean ± standard deviation (SD) using GraphPad Prism 8 (GraphPad Software). The comparison between groups was performed using the *t* test and two-way analysis of variance (ANOVA) test. $P < 0.05$ were considered statistically significant.

■ **RESULTS**

Synthesis and Radiochemistry. HF12, which enables radiolabeling with 68Ga (Figure 1a,b), consists of a 15-amino-acid cyclic peptide conjugated to the metal chelator DOTA. HF12 was synthesized according to the method as shown in
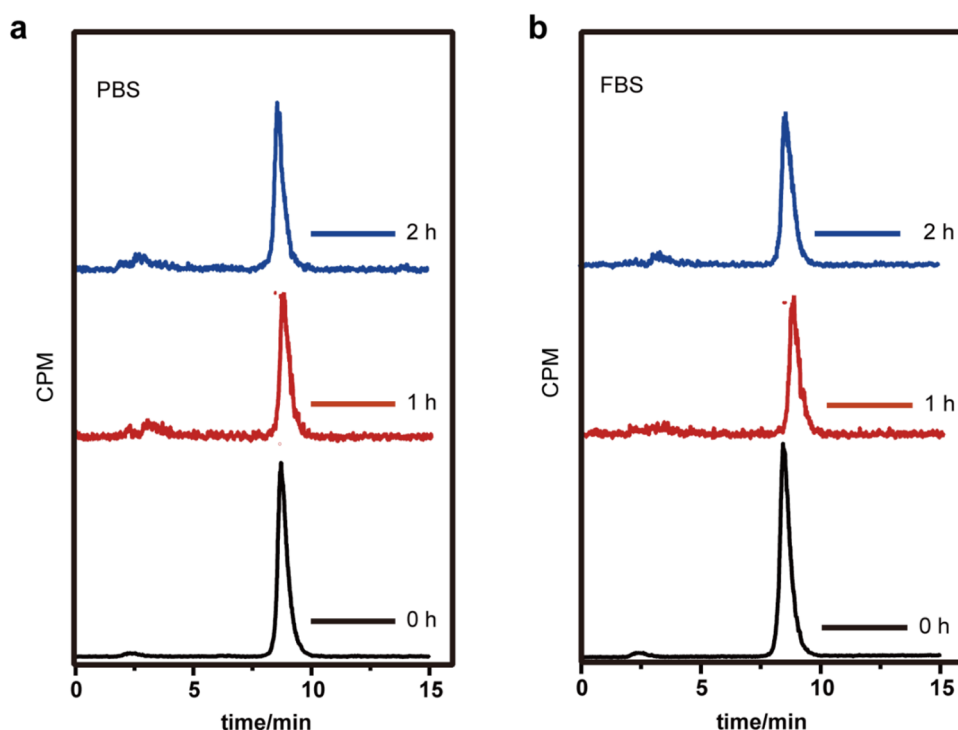
Figure 2. (a) Stability of $[^{68}Ga]HF12$ in PBS. (b) Stability of $[^{68}Ga]HF12$ in FBS.

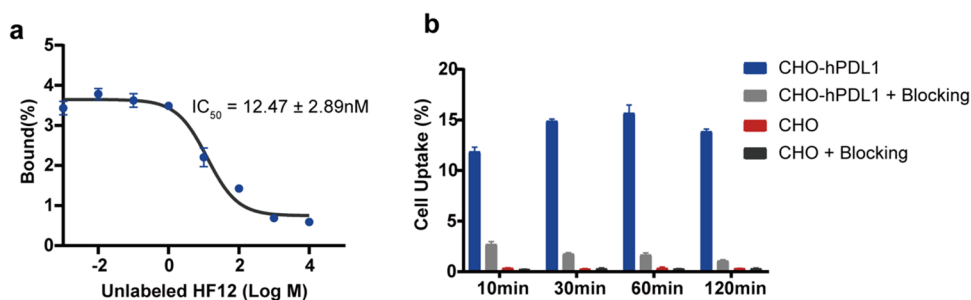**Figure 3.** *In vitro* assay of $[^{68}Ga]HF12$. (a) Competitive binding assay of $[^{68}Ga]HF12$ in CHO-hPD-L1 cells. (b) Uptake of $[^{68}Ga]HF12$ in CHO-hPD-L1 and CHO cells at different time points. The data are presented as mean ± SD.

Supporting Information (Figure S1). HPLC analysis revealed a purity exceeding 95% (Figure S2). The molecular structure of HF12 is $C_{104}H_{150}N_{26}O_{26}S$ (Figure S3).

The radiolabeled complex $[^{68}Ga]HF12$ was synthesized with a radiochemical yield and purity exceeding 95% (Table S2). The molar activity was found to be 8.18 ± 0.25 GBq/μmol (n = 3). The partition coefficient of $[^{68}Ga]HF12$, determined in an octanol−water system, was −1.08 ± 0.02 (n = 3), suggesting significant hydrophilicity. Stability evaluations in PBS, FBS, and *in vivo* were conducted using radio-HPLC. For *in vitro* stability studies, $[^{68}Ga]HF12$ maintained radiochemical purity greater than 90% over 2 h at 37 °C in PBS and FBS (Figure 2a,b). For *in vivo* stability, we assessed post-tail vein injection in mice, and radio-HPLC confirmed a radiochemical purity of over 95% in the bloodstream (Figure S4). These findings indicated that $[^{68}Ga]HF12$ was suitable for further biological evaluations.

Cellular Studies. To ascertain the specificity of $[^{68}Ga]$-HF12 for PD-L1, uptake experiments were conducted in CHO-hPD-L1 and CHO cell lines. The findings demonstrated a time-dependent increase in $[^{68}Ga]HF12$ uptake by CHO-hPD-L1 cells, achieving saturation at 60 min with an uptake of

15.6 ± 0.80%ID/100 μg protein. Conversely, the presence of an excess BMS1166 for blocking markedly reduced $[^{68}Ga]$-HF12 uptake in CHO-hPD-L1 cells, with a peak uptake of 2.71 ± 0.21%ID/100 μg protein observed at 10 min.

Negligible uptake in CHO cells was observed at all time points (Figure 3b). This uptake was consistent with Western blotting, which revealed high PD-L1 expression in CHO-hPD-L1 cells and minimal expression in CHO cells (Figures S7 and S12). Moreover, HF12 effectively inhibited the PD-1:PD-L1 interaction in a dose-dependent manner with an IC_{50} of 12.47 ± 2.89 nM (Figure 3a).

Micro-PET Imaging. Dynamic imaging data (Figures 4b and S5) demonstrated significant uptake of $[^{68}Ga]HF12$ in CHO-hPD-L1 tumors at 10 min post-injection, which increased linearly over time, reaching a maximum uptake of 6.29%ID/g (Figure 4a). The tumor-to-muscle (T/M) ratio in CHO-hPD-L1 tumor-bearing mice was consistently high throughout the 2 h observation period, with a peak value of 4.90%ID/g at 62.5 min. Static scans performed at 1 h post-injection in CHO-hPD-L1 and CHO tumor-bearing mice revealed uptake values of 5.93 ± 0.45 and 3.20 ± 0.40%ID/g in CHO-hPD-L1 and CHO tumors, respectively (Figure 4c,e),
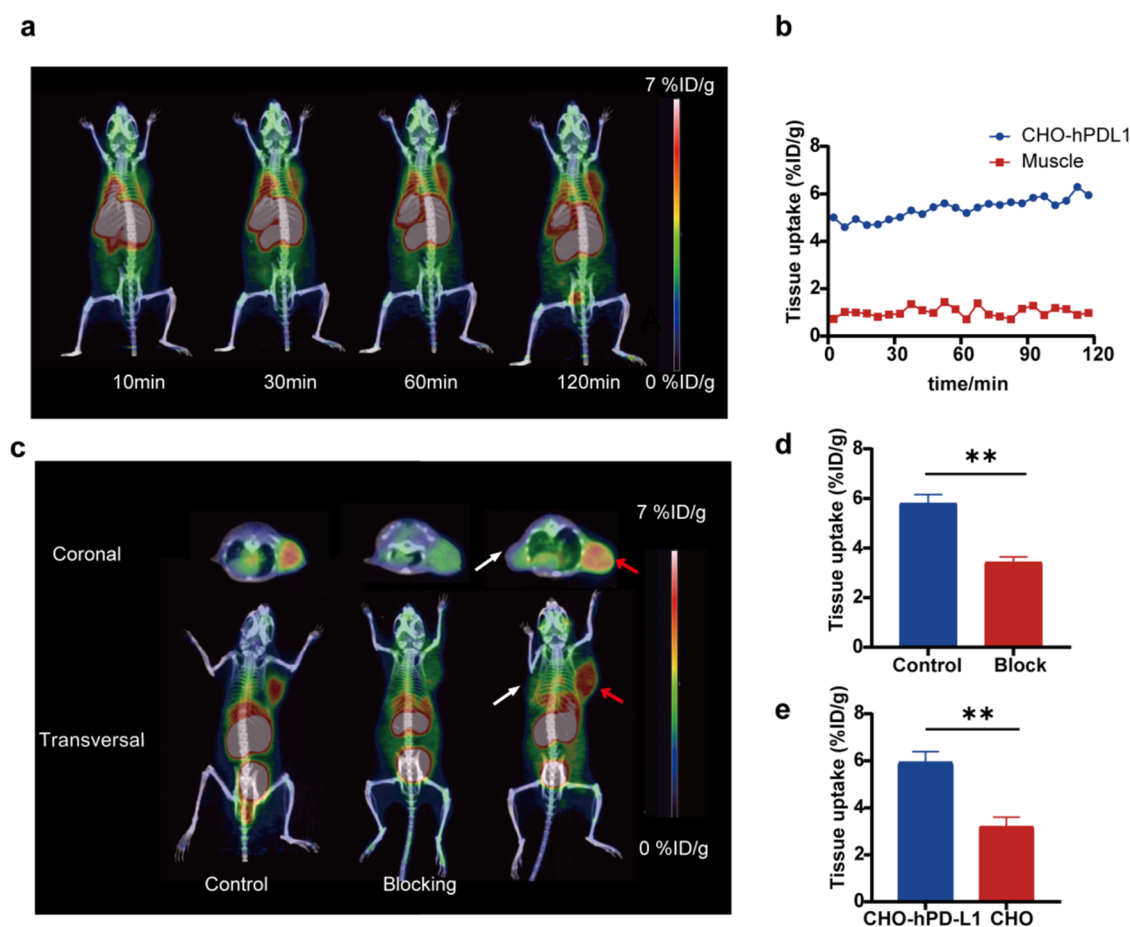
Figure 4. Micro-PET imaging of [^{68}Ga]HF12 in CHO-hPD-L1 and CHO tumor-bearing mice. (a) Representative maximum-intensity projections at 10, 30, 60, and 120 min post-injection of [^{68}Ga]HF12 in CHO-hPD-L1 tumor-bearing mice. (b) Time-activity curves of tumor and muscle uptake in CHO-hPD-L1 tumor-bearing mice. (c) Imaging in CHO-hPD-L1 and CHO tumor-bearing mice at 60 min post-injection of [^{68}Ga]HF12, without (control group) and with (blocking group) co-injection of the inhibitor HF12. (d) Tumor ROI analysis in CHO-hPD-L1 tumor-bearing mice without (control group) or with (blocking group) the inhibitor HF12. (e) Tumor ROI analysis of CHO-hPD-L1 and CHO tumor-bearing mice. CHO-hPD-L1 xenografts were indicated by red arrows, while CHO xenografts were indicated by white arrows. PET images are generated using Inveon Research Workplace software (Siemens) from our own experimental data. Data are presented as mean ± SD, **$P < 0.01$.

with corresponding T/M ratios of 6.49 ± 0.91 and 3.49 ± 0.51.

These findings highlight the ability of [^{68}Ga]HF12 to differentiate tumors based on PD-L1 expression levels. Strikingly, coadministration of excess HF12 significantly reduced the uptake in CHO-hPD-L1 tumors from 5.80 ± 0.36 to 3.43 ± 0.20%ID/g at 60 min (Figure 4c,d), with a corresponding decrease in T/M ratios from 9.41 ± 1.21 to 2.70 ± 0.76. Moreover, substantial tracer accumulation in the kidneys and minimal uptake in the liver were observed, indicative of renal excretion and the hydrophilic nature of the tracer (Figure 4c).

Biodistribution. Biodistribution studies on CHO-hPD-L1 and CHO tumor-bearing mice were performed at 10, 30, 60, and 120 min post-injection (Table S3). The results showed that [^{68}Ga]HF12 was predominantly excreted through the urinary system (Figure 5a). At 1 h post-injection, CHO-hPD-L1 tumors showed the highest uptake at 20.14 ± 2.60%ID/g (Figure 5b), with tumor-to-muscle and tumor-to-blood ratios of 10.34 ± 1.66 and 1.66 ± 0.36 (Figure S6a), respectively. In contrast, PD-L1-negative CHO tumors demonstrated significantly lower uptake of 3.00 ± 0.96%ID/g at the same time point (Figure 5b). Blocking experiments, involving co-injection

with an excess of HF12, reduced uptake in CHO-hPD-L1 tumors to 5.91 ± 1.04%ID/g, thereby confirming the specificity of HF12 for PD-L1 expression (Figure 5b). At 2 h post-injection, the uptake in CHO-hPD-L1 tumors decreased to 11.56 ± 3.18%ID/g, while the tumor-to-muscle and tumor-to-blood ratios had increased to 18.93 ± 9.35 and 2.61 ± 0.78, respectively (Figures 5a and S6b).

In vivo autoradiography further validated the tumor uptake of [^{68}Ga]HF12, and IHC confirmed PD-L1 expression in the tumors (Figure 5c).

Monitoring the Efficacy of Monoclonal Antibody Treatment. Micro-PET imaging with [^{68}Ga]HF12 was utilized to assess the immunotherapeutic effects of Atezolizumab, with PBS treatment serving as a negative control. Static imaging was performed at 1 h after intravenous injection of [^{68}Ga]HF12 in CHO-hPD-L1 tumor-bearing mice, both before and after treatment with Atezolizumab and PBS (Figure 6a). Before Atezolizumab administration, [^{68}Ga]HF12 exhibited high tumor accumulation, with a mean uptake of 5.33 ± 0.25%ID/g and a tumor-to-muscle (T/M) ratio of 7.72 ± 0.48, as depicted in Figures 6b,6e and S8a. After two treatments of Atezolizumab (Group B), there was a notable reduction in the [^{68}Ga]HF12 signal intensity at the tumor site,
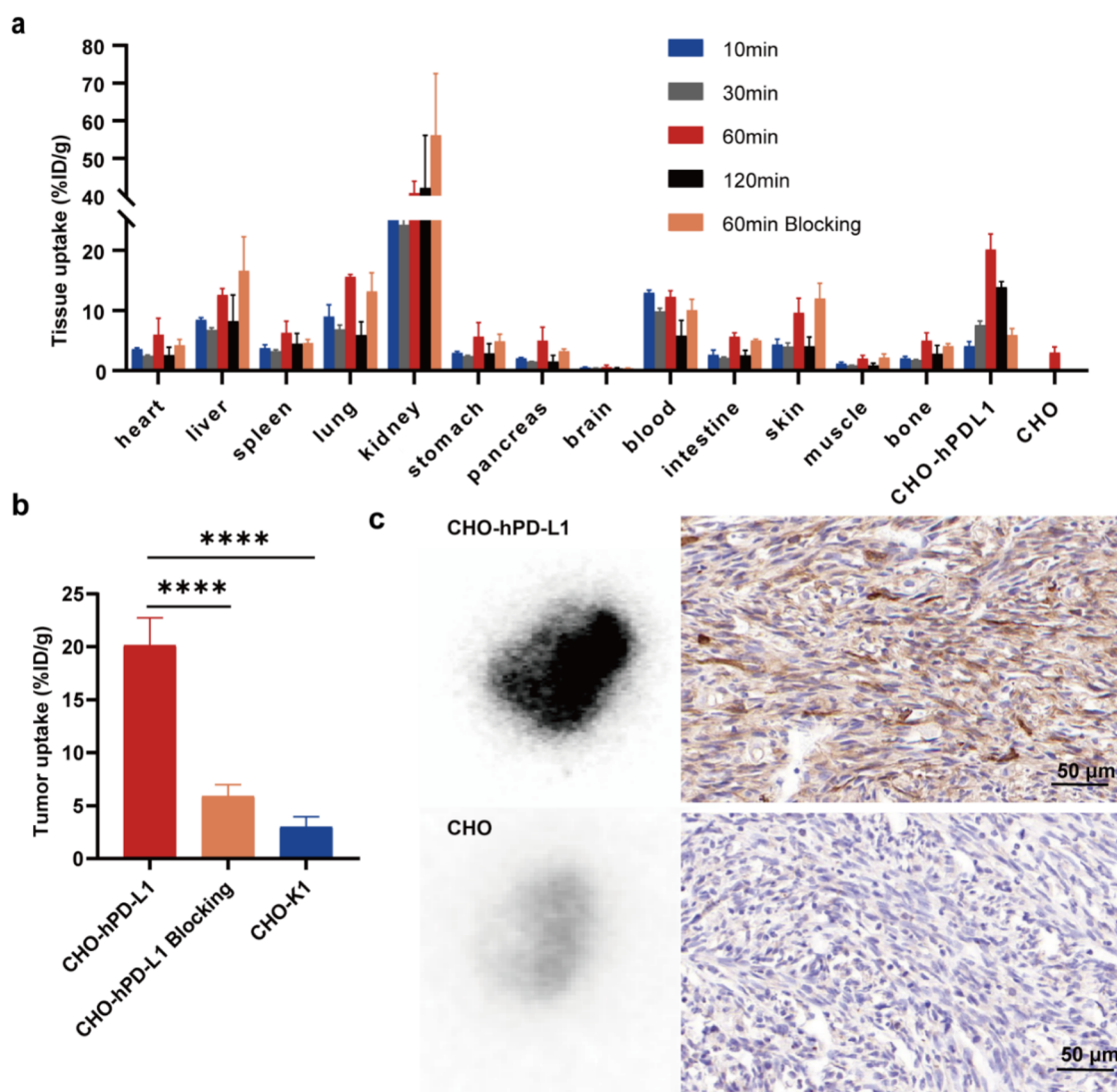
Figure 5. Biodistribution of [68Ga]HF12 in tumor-bearing mice. (a) Biodistribution at different time points in CHO-hPD-L1 and CHO tumor-bearing mouse models ($n = 3$) after intravenous injection of [68Ga]HF12. (b) Comparison of the biodistribution in tumor tissues of CHO-hPD-L1 mice co-injected without or with inhibitor HF12 and CHO tumor-bearing mice. (c) *In vivo* autoradiography and PD-L1 immunohistochemistry of CHO-hPD-L1 and CHO tumor tissues. Data are presented as mean ± SD, ****$P < 0.0001$.

with uptake decreasing to 3.2 ± 0.17%ID/g and a tumor-to-muscle (T/M) ratio of 3.50 ± 0.43, suggesting a reduced availability of PD-L1 binding sites (Figures 6b,6e and S8a). Following five treatments, tumor uptake stabilized at 3.16 ± 0.15%ID/g and a T/M ratio of 2.55 ± 0.50 (Figures 6b,e and S8a). In the control group, tumor uptake showed no significant variation before or after PBS treatment (Group A). The [68Ga]HF12 uptake in CHO-hPD-L1 tumor-bearing mice remained consistent at 5.46 ± 1.07%ID/g before treatment and 6.00 ± 1.15 and 5.90 ± 1.08%ID/g after two and five PBS treatments, respectively, with T/M ratios maintaining at 6.82 ± 0.65, 6.10 ± 0.64, and 6.83 ± 1.89, respectively (Figures 6b,e and S8a).

To confirm the binding of Atezolizumab to PD-L1 in tumors, biodistribution studies of [68Ga]HF12 were conducted in CHO-hPD-L1 tumor-bearing mice after treatment (Table S4). Results showed that PBS-treated (Group A) mice exhibited high radioactivity accumulation (7.83 ± 0.22%ID/g) in tumors, whereas Atezolizumab-treated mice displayed significantly lower tracer uptake (3.70 ± 0.06%ID/g, Figures

7a and S8b). These findings were consistent with previous CHO tumor-bearing mice biodistribution data, suggesting near-saturation of PD-L1 targets in the tumors after Atezolizumab treatment.

Throughout the treatment period, tumor volumes and body weights of the mice were monitored every 3 days. Comparison between the Atezolizumab and PBS groups revealed no significant differences in tumor volume until the fourth measurement, where Atezolizumab began to demonstrate its inhibitory effect (Figure 6d). Additionally, no notable differences in body weight were detected between the two groups (Figure 6c). In summary, [68Ga]HF12 demonstrated both sensitivity and specificity in assessing Atezolizumab's targeting of PD-L1 expression at the tumor site.

Quantifying Dynamic Changes in PD-L1 after Immunotherapy. To further investigate the capacity of [68Ga]HF12 to monitor dynamic changes in tumor PD-L1 expression post-immunotherapy, Western blotting and IHC were conducted on tumors collected post-treatment. The results revealed a substantial reduction of approximately 70%
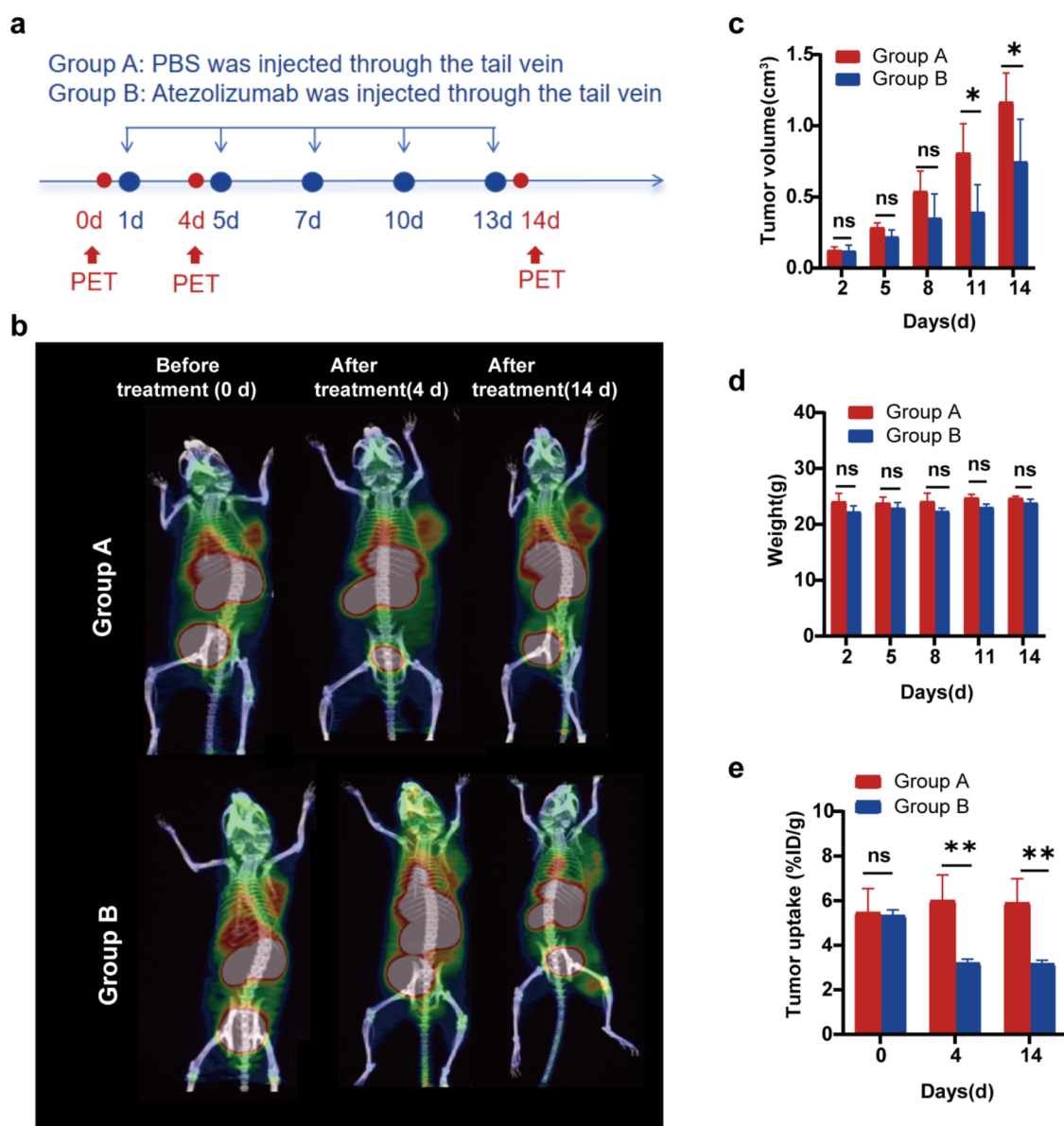
Figure 6. Monitoring of treatment in CHO-hPD-L1 tumor-bearing mice following administration of PBS and Atezolizumab. (a) Experimental design. (b) Micro-PET imaging of CHO-hPD-L1 tumor-bearing mice injected with [^{68}Ga]HF12 at 60 min after different treatment times with PBS and Atezolizumab. (c) Changes in tumor volume of CHO-hPD-L1 tumor-bearing mice during treatment. (d) Changes in body weight over time in CHO-hPD-L1 tumor-bearing mice during treatment. (e) PET imaging uptake of tumors in the PBS group and Atezolizumab group at different treatment times. PET images are generated using Inveon Research Workplace software (Siemens) from our own experimental data. Data are presented as mean ± SD, "NS" indicates no statistically significant difference between groups. *$P < 0.05$, **$P < 0.01$.

in PD-L1 expression in tumors from mice treated with Atezolizumab compared to the PBS group (Figures S9 and S13), aligning with the trends observed above micro-PET imaging and biodistribution studies. More importantly, as depicted in Figure S10, the uptake of tumors in PET images is well correlated with the expression of PD-L1 detected by Western blotting analysis ($R^2 = 0.9632$, $P < 0.0001$). IHC analysis revealed significantly higher tumor staining intensity in the PBS-treated group compared to that in the Atezolizumab-treated group (Figure 7b). These findings validated the efficacy of [^{68}Ga]HF12 in monitoring alterations in PD-L1 expression induced by immunotherapy. In summary, [^{68}Ga]HF12 exhibited the potential to monitor the dynamic variations in PD-L1 expression levels post-immunotherapy.

To assess any potential damage caused by Atezolizumab to normal tissues, HE staining on the heart, liver, spleen, lungs, and kidneys from both treatment groups was performed after the treatment period. No histopathological abnormalities were detected in the major organs of mice treated with Atezolizumab or PBS (Figure S11), indicating the absence of significant toxicological repercussions associated with Atezolizumab immunotherapy in this murine model.

■ DISCUSSION

Immunotherapy targeting the PD-1/PD-L1 pathway has shown significant clinical efficacy. Radiolabeled PD-L1 tracers provide a quantitative approach to evaluate PD-L1 expression, which is instrumental in identifying patients who may respond favorably to immunotherapeutic strategies. In this context, we
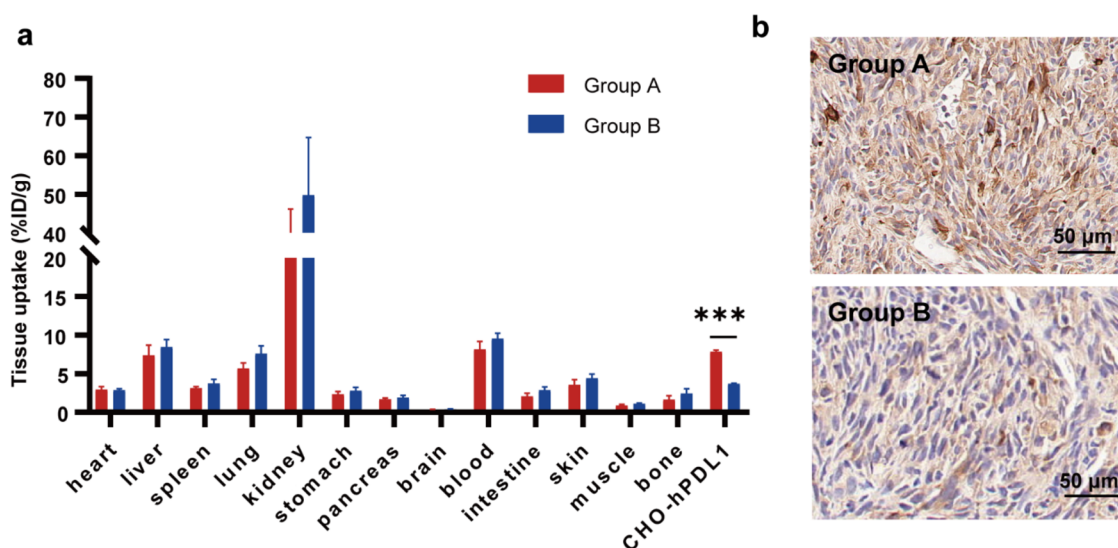
Figure 7. Biodistribution and IHC of $[^{68}Ga]$HF12 in CHO-hPD-L1 tumor-bearing mice following administration of PBS and Atezolizumab. Group A was treated with PBS, while Group B received the anti-PD-L1 antibody Atezolizumab. (a) Biodistribution of $[^{68}Ga]$HF12 in CHO-hPD-L1 tumor-bearing mice at 60 min post-injection after PBS and Atezolizumab treatment. (b) PD-L1 immunohistochemistry in tumor tissues after treatment with PBS and Atezolizumab. Data are presented as mean ± SD, ***$P < 0.001$.

synthesized a high-affinity tracer, $[^{68}Ga]$HF12, specifically designed to target PD-L1. This tracer is intended to monitor dynamic changes in PD-L1 expression after immunotherapy and can be utilized to assess the inhibitory efficacy of immunotherapy on PD-L1 levels.

HF12 exhibited an IC_{50} of 12.47 ± 2.89 nM. Following radiolabeling, $[^{68}Ga]$HF12 maintained notable stability both *in vitro* and *in vivo* throughout the incubation period, establishing a solid foundation for further investigations. In cellular uptake assays, $[^{68}Ga]$HF12 showed markedly higher uptake in PD-L1-positive CHO-hPD-L1 cells compared with PD-L1-negative CHO cells, indicating selective uptake by PD-L1-expressing cells. Moreover, the uptake of $[^{68}Ga]$HF12 in CHO-hPD-L1 cells was notably inhibited by the PD-L1 small-molecule inhibitor BMS1166, further validating the specificity of $[^{68}Ga]$HF12 for PD-L1.

In PET imaging and biodistribution studies, the tracer rapidly accumulated in tumors with high PD-L1 expression in a short period, with the tumor-to-muscle ratio remaining elevated over a 2 h period. PD-L1-negative CHO tumors exhibited minimal uptake, which was not significantly different from the uptake observed in CHO-PD-L1 tumors following blockade with HF12. Furthermore, owing to the hydrophilic properties of HF12, the tracer was mainly excreted *via* the kidneys with limited hepatic uptake, thereby facilitating the acquisition of high-contrast images. In contrast, radiolabeled WL12 exhibited high liver uptake, which may compromise imaging quality in abdominal tumors.[19,22]

Given the inflammatory response induced by immunotherapy, which can lead to increased tumor uptake, $[^{18}F]$FDG has certain limitations in monitoring such therapies.[27,28] In this study, we also validated the use of $[^{68}Ga]$HF12 in monitoring the dynamic changes in PD-L1 expression levels post-immunotherapy. Atezolizumab was chosen for this investigation due to its long half-life, strong affinity, and status as the first FDA-approved PD-L1 monoclonal antibody.

After two treatments of Atezolizumab, PET imaging showed a significant reduction in the standardized uptake value (SUV) of the tumor lesions, while there was no notable difference in tumor uptake before and after treatment in the PBS control group. Additionally, post-treatment assessments confirmed a decrease in PD-L1 expression in Atezolizumab-treated tumors by Western blotting and IHC, aligned with the PET imaging results. These findings indicated that PD-L1 expression levels declined in tumors following Atezolizumab treatment and that $[^{68}Ga]$HF12 was capable of dynamically monitoring these changes. However, in the biodistribution evaluating the efficacy of monoclonal antibody treatment, we observed a reduced tumor uptake of $[^{68}Ga]$HF12 in the PBS group compared to the group that did not receive administration in prior biodistribution experiments. This difference may be attributable to the variations in the stages of tumor progression among the mice used for imaging in the two experiments. In the PBS group, the tumors had already undergone partial necrosis, which could have resulted in decreased radiotracer accumulation. Additionally, the use of different batches of mice across these two experiments could have introduced potential confounding variables.

However, it was important to note that Atezolizumab did not significantly inhibit tumor growth, potentially due to inadequate monoclonal antibody dose, variability in tumor types, or potentially low PD-L1 expression levels. Furthermore, this study employed NOD/SCID mice, which exhibit immunodeficiencies in both T and B cells. The recognition and elimination of tumor cells by the organism are predominantly mediated by cytotoxic T cells.[29,30]

CONCLUSIONS

In summary, this study introduced the development of a novel peptide-based radiotracer, $[^{68}Ga]$HF12, which is specifically designed for the detection of PD-L1 expression in cellular and animal models. $[^{68}Ga]$HF12 demonstrated a high affinity for PD-L1, efficiently and selectively identifying tumors with diverse PD-L1 expression levels and exhibiting a rapid uptake in tumor tissues. Moreover, $[^{68}Ga]$HF12 was capable of quantifying dynamic changes in PD-L1 expression levels, thereby facilitating the prediction and monitoring of responses to anti-PD-1 and anti-PD-L1 immunotherapies. Consequently,

[^{68}Ga]HF12 holds significant promise for future clinical research in immunotherapy.

■ ASSOCIATED CONTENT

Data Availability Statement
All data generated or analyzed during this study are included in this published article and its Supporting Information.

Ⓢ Supporting Information
The Supporting Information is available free of charge at https://pubs.acs.org/doi/10.1021/acsomega.4c11396.

General procedure for the preparation of HF12; chemical structure formula of HF12; HPLC trace and LC-MS of HF12; result of *in vivo* stability; time-activity curves from dynamic imaging; tumor-to-nontarget organ ratios in biodistribution studies; Western blot analysis; tumor-to-muscle ratio after immunotherapy; Western blot analysis in different groups; the relevance between uptake and PD-L1 expression; H&E staining of normal tissues; HPLC conditions and radiochemical purity; and biodistribution data (PDF)

■ AUTHOR INFORMATION

Corresponding Authors
Xiangsong Zhang − *Department of Nuclear Medicine, The First Affiliated Hospital of Sun Yat-sen University, Guangzhou 510080 Guangdong, China;* Phone: +8613711471890; Email: zhxiangs@mail.sysu.edu.cn; Fax: +86-020-87766335

Zhihao Zha − *Department of Nuclear Medicine, The First Affiliated Hospital of Sun Yat-sen University, Guangzhou 510080 Guangdong, China;* ⓞ orcid.org/0009-0000-5360-3962; Phone: +8617319488127; Email: zhazhh@mail.sysu.edu.cn; Fax: +86-020-87766335

Authors
Hui Nie − *Department of Nuclear Medicine, The First Affiliated Hospital of Sun Yat-sen University, Guangzhou 510080 Guangdong, China*

Lei Peng − *Department of Ultrasound Medicine, The First People's Hospital of FoShan, Foshan 528000 Guangdong, China*

Tianhong Yang − *Department of Nuclear Medicine, The First Affiliated Hospital of Sun Yat-sen University, Guangzhou 510080 Guangdong, China*

Junyu Chen − *College of Environmental Science and Engineering, North China Electric Power University, Beijing 102206, China*

Chengde Xie − *College of Environmental Science and Engineering, North China Electric Power University, Beijing 102206, China*

Lingyu Xue − *Department of Nuclear Medicine, The First Affiliated Hospital of Sun Yat-sen University, Guangzhou 510080 Guangdong, China*

Dake Zhang − *Department of Nuclear Medicine, The First Affiliated Hospital of Sun Yat-sen University, Guangzhou 510080 Guangdong, China*

Renbo Wu − *Department of Nuclear Medicine, The First Affiliated Hospital of Sun Yat-sen University, Guangzhou 510080 Guangdong, China*

Complete contact information is available at:
https://pubs.acs.org/10.1021/acsomega.4c11396

Author Contributions
Conception and design: Z.Z. and X.Z.; acquisition of data: H.N., L.P., T.Y., J.C., C.X., L.X.; technical support: Z.Z., D.Z., R.W.; analysis and interpretation of data: Z.Z., X.Z., H.N., L.P., T.Y., J.C., C.X., L.X.; writing the manuscript: H.N.; revision of the manuscript: T.Y., Z.Z., and X.Z.

Notes
The authors declare no competing financial interest.

Ethics Approval All animal care and experimental procedures were performed following the guidelines of the care and use of laboratory animals approved by the First Affiliated Hospital of Sun Yat-sen University Institutional Animal Care and Use Committee.

■ ACKNOWLEDGMENTS

■ ABBREVIATIONS

PD-1, programmed death protein 1; PD-L1, programmed death-ligand 1; PET, positron emission tomography; IHC, immunohistochemical; PBS, phosphate-buffered saline; SPECT, single photon emission computed tomography; HCl, hydrochloric acid; HPLC, high-performance liquid chromatography; DMSO, dimethyl sulfoxide; FBS, fetal bovine serum; P/S, penicillin−streptomycin solution; NaOH, sodium hydroxide; ROIs, regions of interest; SUV, standardized uptake value

■ REFERENCES

(1) Chen, G.; Huang, A. C.; Zhang, W.; Zhang, G.; Wu, M.; Xu, W.; Yu, Z.; Yang, J.; Wang, B.; Sun, H.; et al. Exosomal PD-L1 contributes to immunosuppression and is associated with anti-PD-1 response. *Nature* **2018**, *560* (7718), 382−386.

(2) Gajewski, T. F.; Schreiber, H.; Fu, Y. X. Innate and adaptive immune cells in the tumor microenvironment. *Nat. Immunol.* **2013**, *14* (10), 1014−1022.

(3) Hamanishi, J.; Mandai, M.; Matsumura, N.; Abiko, K.; Baba, T.; Konishi, I. PD-1/PD-L1 blockade in cancer treatment: perspectives and issues. *Int. J. Clin. Oncol.* **2016**, *21* (3), 462−473.

(4) Sunshine, J.; Taube, J. M. PD-1/PD-L1 inhibitors. *Curr. Opin. Pharmacol.* **2015**, *23*, 32−38.

(5) Brody, R.; Zhang, Y.; Ballas, M.; Siddiqui, M. K.; Gupta, P.; Barker, C.; Midha, A.; Walker, J. PD-L1 expression in advanced NSCLC: Insights into risk stratification and treatment selection from a systematic literature review. *Lung Cancer* **2017**, *112*, 200−215.

(6) Patel, S. P.; Kurzrock, R. PD-L1 Expression as a Predictive Biomarker in Cancer Immunotherapy. *Mol. Cancer Ther.* **2015**, *14* (4), 847−856.

(7) Büttner, R.; Gosney, J. R.; Skov, B. G.; Adam, J.; Motoi, N.; Bloom, K. J.; Dietel, M.; Longshore, J. W.; Lopez-Rios, F.; Penault-Llorca, F.; et al. Programmed Death-Ligand 1 Immunohistochemistry Testing: A Review of Analytical Assays and Clinical Implementation in Non-Small-Cell Lung Cancer. *J. Clin. Oncol.* **2017**, *35* (34), 3867−3876.

(8) Nimmagadda, S. Quantifying PD-L1 Expression to Monitor Immune Checkpoint Therapy: Opportunities and Challenges. *Cancers* **2020**, *12* (11), No. 3173.

(9) Crişan, G.; Moldovean-Cioroianu, N. S.; Timaru, D.-G.; Andries, G.; Cainap, C.; Chis, V. Radiopharmaceuticals for PET and SPECT Imaging: A Literature Review over the Last Decade. *Int. J. Mol. Sci.* **2022**, *23* (9), No. 5023.

(10) Maute, R. L.; Gordon, S. R.; Mayer, A. T.; McCracken, M. N.; Natarajan, A.; Ring, N. G.; Kimura, R.; Tsai, J. M.; Manglik, A.; Kruse, A. C.; et al. Engineering high-affinity PD-1 variants for optimized immunotherapy and immuno-PET imaging. *Proc. Natl. Acad. Sci. U.S.A.* **2015**, *112* (47), E6506−E6514.

(11) Niemeijer, A. N.; Leung, D.; Huisman, M. C.; Bahce, I.; Hoekstra, O. S.; van Dongen, G. A. M. S.; Boellaard, R.; Du, S.; Hayes, W.; Smith, R.; et al. Whole body PD-1 and PD-L1 positron emission tomography in patients with non-small-cell lung cancer. *Nat. Commun.* **2018**, *9* (1), No. 4664.

(12) Chen, Y.; Guo, Y.; Liu, Z.; Hu, X.; Hu, M. An overview of current advances of PD-L1 targeting immuno-imaging in cancers. *J. Cancer Res. Ther.* **2023**, *19* (4), 866−875.

(13) Bensch, F.; van der Veen, E. L.; Lub-de Hooge, M. N.; Jorritsma-Smit, A.; Boellaard, R.; Kok, I. C.; Oosting, S. F.; Schroder, C. P.; Hiltermann, T. J. N.; van der Wekken, A. J.; et al. ⁸⁹Zr-atezolizumab imaging as a non-invasive approach to assess clinical response to PD-L1 blockade in cancer. *Nat. Med.* **2018**, *24* (12), 1852−1858.

(14) Massicano, A. V. F.; Song, P. N. N.; Mansur, A.; White, S. L.; Sorace, A. G.; Lapi, S. E. ⁸⁹Zr-Atezolizumab-PET Imaging Reveals Longitudinal Alterations in PDL1 during Therapy in TNBC Preclinical Models. *Cancers* **2023**, *15* (10), No. 2708.

(15) Vento, J.; Mulgaonkar, A.; Woolford, L.; Nham, K.; Christie, A.; Bagrodia, A.; de Leon, A. D.; Hannan, R.; Bowman, I.; McKay, R. M.; et al. PD-L1 detection using ⁸⁹Zr-atezolizumab immuno-PET in renal cell carcinoma tumorgrafts from a patient with favorable nivolumab response. *J. Immunother. Cancer* **2019**, *7* (1), No. 144.

(16) Bouleau, A.; Nozach, H.; Dubois, S.; Kereselidze, D.; Chevaleyre, C.; Wang, C.-I.; Evans, M. J.; Lebon, V.; Maillere, B.; Truillet, C. Optimizing Immuno-PET Imaging of Tumor PD-L1 Expression: Pharmacokinetic, Biodistribution, and Dosimetric Comparisons of ⁸⁹Zr-Labeled Anti-PD-L1 Antibody Formats. *J. Nucl. Med.* **2022**, *63* (8), 1259−1265.

(17) Jung, K.-H.; Park, J. W.; Lee, J. H.; Moon, S. H.; Cho, Y. S.; Lee, K.-H. ⁸⁹Zr-Labeled Anti-PD-L1 Antibody PET Monitors Gemcitabine Therapy-Induced Modulation of Tumor PD-L1 Expression. *J. Nucl. Med.* **2021**, *62* (5), 656−664.

(18) Li, D.; Cheng, S.; Zou, S.; Zhu, D.; Zhu, T.; Wang, P.; Zhu, X. Immuno-PET Imaging of ⁸⁹Zr Labeled Anti-PD-L1 Domain Antibody. *Mol. Pharmaceutics* **2018**, *15* (4), 1674−1681.

(19) De Silva, R. A.; Kumar, D.; Lisok, A.; Chatterjee, S.; Wharram, B.; Rao, K. V.; Mease, R.; Dannals, R. F.; Pomper, M. G.; Nimmagadda, S. Peptide-Based ⁶⁸Ga-PET Radiotracer for Imaging PD-L1 Expression in Cancer. *Mol. Pharmaceutics* **2018**, *15* (9), 3946−3952.

(20) Zhou, X.; Jiang, J.; Yang, X.; Liu, T.; Ding, J.; Nimmagadda, S.; Pomper, M. G.; Zhu, H.; Zhao, J.; Yang, Z.; Li, N. First-in-Humans Evaluation of a PD-L1-Binding Peptide PET Radiotracer in Non-Small Cell Lung Cancer Patients. *J. Nucl. Med.* **2022**, *63* (4), 536−542.

(21) Chatterjee, S.; Lesniak, W. G.; Miller, M. S.; Lisok, A.; Sikorska, E.; Wharram, B.; Kumar, D.; Gabrielson, M.; Pomper, M. G.; Gabelli, S. B.; Nimmagadda, S. Rapid PD-L1 detection in tumors with PET using a highly specific peptide. *Biochem. Biophys. Res. Commun.* **2017**, *483* (1), 258−263.

(22) Kumar, D.; Lisok, A.; Dahmane, E.; McCoy, M.; Shelake, S.; Chatterjee, S.; Allaj, V.; Sysa-Shah, P.; Wharram, B.; Lesniak, W. G.; et al. Peptide-based PET quantifies target engagement of PD-L1 therapeutics. *J. Clin. Invest.* **2019**, *129* (2), 616−630.

(23) Holt, D. P.; Kumar, D.; Nimmagadda, S.; Dannals, R. F. An optimized radiosynthesis of ¹⁸F DK222, a PET radiotracer for imaging PD-L1. *J. Labelled Compd. Radiopharm.* **2023**, *66* (2), 47−54.

(24) Mishra, A.; Gupta, K.; Kumar, D.; Lofland, G.; Sharma, A. K.; Solnes, L. B.; Rowe, S. P.; Forde, P. M.; Pomper, M. G.; Gabrielson, E. W.; Nimmagadda, S. Non-invasive PD-L1 quantification using ¹⁸F DK222-PET imaging in cancer immunotherapy. *J. Immunother. Cancer* **2023**, *11* (10), No. e007535.

(25) Mishra, A.; Kumar, D.; Gupta, K.; Lofland, G.; Sharma, A. K.; Banka, D. S.; Hobbs, R. F.; Dannals, R. F.; Rowe, S. P.; Gabrielson, E.; Nimmagadda, S. Gallium-68-labeled Peptide PET Quantifies Tumor Exposure of PD-L1 Therapeutics. *Clin. Cancer Res.* **2023**, *29* (3), 581−591.

(26) Monaco, L.; De Bernardi, E.; Bono, F.; Cortinovis, D.; Crivellaro, C.; Elisei, F.; L'Imperio, V.; Landoni, C.; Mathoux, G.; Musarra, M.; et al. The ″digital biopsy″ in non-small cell lung cancer (NSCLC): a pilot study to predict the PD-L1 status from radiomics features of ¹⁸F FDG PET/CT. *Eur. J. Nucl. Med. Mol. Imaging* **2022**, *49* (10), 3401−3411.

(27) Groheux, D.; Hindie, E.; Tredaniel, J.; Giraudet, A. L.; Vaylet, F.; Berenger, N.; Moretti, J. L. PET-CT for evaluation of the solitary pulmonary nodule: an update. *Rev. Mal. Respir.* **2009**, *26* (10), 1041−1055.

(28) Long, N. M.; Smith, C. S. Causes and imaging features of false positives and false negatives on F-PET/CT in oncologic imaging. *Insights Imaging* **2011**, *2* (6), 679−698.

(29) Ai, L.; Xu, A.; Xu, J. Roles of PD-1/PD-L1 Pathway: Signaling, Cancer, and Beyond. *Adv. Exp. Med. Biol.* **2020**, *1248*, 33−59.

(30) Lau, J.; Cheung, J.; Navarro, A.; Lianoglou, S.; Haley, B.; Totpal, K.; Sanders, L.; Koeppen, H.; Caplazi, P.; McBride, J.; et al. Tumour and host cell PD-L1 is required to mediate suppression of anti-tumour immunity in mice. *Nat. Commun.* **2017**, *8*, No. 14572.